Reports

New Evidence on the Size and Possible Effects of a Late Pliocene Oceanic Asteroid Impact

FRANK T. KYTE, LEI ZHOU, JOHN T. WASSON

Debris from a late Pliocene asteroid impact is spread across at least 600 kilometers of the ocean floor in the southeast Pacific. On the basis of iridium concentrations in sediments from six deep-sea cores, the asteroid diameter was at least 0.5 kilometer; the impacting projectile may have been one of the largest in the last few million years. The stratigraphic age of this impact is the same as that inferred for the onset of Northern Hemisphere glaciation.

IN 1981 WE REPORTED (*1*) THAT ANOMalously high noble metal and meteoritic particle concentrations occur in upper Pliocene (~2.3 Ma) sediments from deep-sea piston core E13-3, which was recovered from the southeast Pacific about 1400 km west of Cape Horn. In a later study Kyte and Brownlee showed (*2*) that the millimeter-sized meteoritic particles consist largely of Ir-rich impact melt, but a few percent are unmelted meteoritic fragments; a few metal grains were also found. The isotopic, mineralogical, and chemical compositions of the particles indicate that the projectile was a low-metal mesosiderite meteorite. Chemical analyses also indicate that oceanic crustal material did not contaminate the impact melt, which appears to be asteroidal material diluted only by a minor amount of sea salt. It appears that the impact was into the local deep (~5 km) ocean basin and did not produce a crater on the ocean floor (*2*).

To better assess the mass of the impactor, we have studied five additional cores from the region (Fig. 1). These sections (*3*) were analyzed for Ir (*4*); some coarse fractions were searched for the presence of impact debris (*5*). The highest Ir concentrations occur in E13-4 (Fig. 2), the locality farthest west. Maximum Ir concentrations are 20 ng/g in E13-4, 5 ng/g in E13-3, 1.2 ng/g in E10-2, and 0.8 ng/g in E13-1 (Fig. 2). Maximum Ir concentrations in the other two sections (*3*) are 0.5 ng/g in E13-6 and 0.25 ng/g in E13-7, too low to confirm the presence of an impact deposit (*6*).

The upper Pliocene horizon in E13-4 has Ir concentrations comparable to those in the Cretaceous-Tertiary (KT) boundary layer. In contrast to the case for the KT boundary, the late Pliocene projectile has been positively identified (on the basis of the composition of the meteoritic debris) as an asteroid rather than a comet. This is also the only known impact into a deep-ocean basin, and, unlike other impact horizons, the chief Ir-bearing carrier (the impact melt) has been separated.

Concentrations of impact-melt debris at these sites are roughly proportional to Ir concentration. The maximum impact melt concentration is ~10% by dry mass in E13-4, 2% in E13-3, and 0.1% in E10-2. Impact debris was not found in E13-1 (*7*). Elevated Ir concentrations at each locality extend across at least 30 cm of section (Fig. 2). Bioturbation and possibly also some reworking of fine-grained impact debris by bottom currents may have smeared an initially thin horizon.

The high concentrations of Ir and meteoritic particles in E13-4 and E13-3 indicate that the asteroid impacted near these sites. Impact into the ocean would certainly have resulted in vaporization of a large fraction of the projectile and shock melting of most of the remainder. Fragments dispersed during infall may have decelerated in the atmosphere and provided the unmelted projectile material. After the impact, coarse particles would have settled out near the site of splashdown, but fine particles and vesicular impact melt materials would have settled slowly and may have been transported some distance by ocean currents.

Iridium concentrations range from 130 to 260 ng/g in 26 impact melt particles from E13-3 and E13-4. Particles from E13-3 tend to have slightly (~15%) lower Ir concentrations and seem to be more altered than particles from E13-4. Impact-melt particles account for ~40% of the Ir in both E13-3 and E13-4. If we assume that all of the Ir was originally in the coarse particles, the asteroid could have no more Ir than 500 ng/g. Our best estimate for the Ir concentration of the asteroid is the mean of the highest 30% of the Ir contents, 240 ng/g. Using this value, we can estimate the amount of asteroidal debris deposited at each site from the Ir fluence.

We estimated (*1*) that the minimum diameter of the impacting asteroid was >20 m on the basis of the E13-3 data. With the discovery of impact melt particles in E13-4, Kyte and Brownlee increased the estimate of the diameter to 100 to 500 m (*2*). In this study we have shown that the E13-4 impact deposit [missed by Kyte and Brownlee (*2*)] contains ~100 times as much debris as they estimated. With Ir data on E13-4 and four additional cores we can now better define the fallout pattern and thus improve the accuracy of the estimate for the size of the asteroid.

In modeling the fallout distribution we assumed that the fallout pattern will be lengthened by oceanic and atmospheric currents, both of which are toward the east at this latitude, a circulation pattern that has probably persisted since at least the late Miocene (*8*). We considered concentric circular and ellipsoidal fallout distributions, but the lowest (and thus most conservative) estimate of projectile mass was obtained by modeling the concentration contours with a series of coaxial ellipses with the ellipse centers moving east-northeast from E13-4 toward E10-2 with decreasing Ir concentration (Fig. 3). The b/a ratio of the ellipses was visually fit to be 0.75; a was increased by factors of 1.6 and the new center was offset east-northeast by 0.3 a from the previous center. Contour concentrations were assigned on the basis of the data from the cores. We integrated these contours by assuming that the mean concentration in the areas between contours is 1.2 times the concentration of the outer (lower) contour

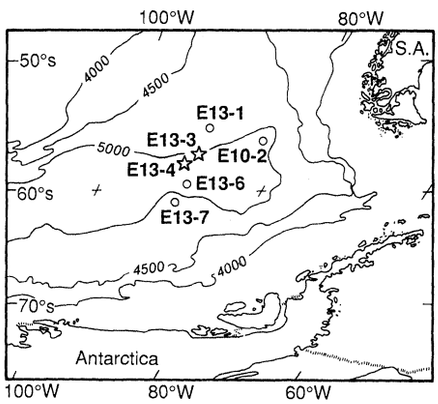

Fig. 1. Location map for USNS *Eltanin* piston cores used in this study. Significant enhancements in Ir concentration are observed in cores E13-3, E13-4, E10-2, and E13-1, and extraterrestrial particles have been found in all of these but E13-1. The high Ir and particle concentrations in E13-3 and E13-4 indicate that these sites were closest to the impact. Bathymetry is in meters; S.A. is South America.

Institute of Geophysics and Planetary Physics, University of California, Los Angeles, CA 90024.

and by assuming that the Ir fluence is 5 ng/cm^2 in a region exterior to the contours with an area equal to that of the outer ellipse. This method yields a total Ir fluence of 6×10^{16} ng, which corresponds to a projectile mass of 2.5×10^{14} g and a diameter of 500 m (for a density of 3.5 g/cm^3). For a velocity of 20 km/s, this corresponds to a kinetic energy of 5×10^{19} J, equivalent to the explosive power of 12 gigatons of TNT.

This mass estimate does not include projectile materials scattered over greater distances. Analogies with nuclear weapons tests suggest that 50% or more of the projectile material could have been injected into the stratosphere (*9*). Depending on the nature of the explosion, up to 50% of the ejected material could have been dispersed into the Northern Hemisphere. Thus inclusion of fallout from outside the local region would yield a projectile mass two or more times as large.

Given the available data, we propose that the diameter of the asteroid was at least 0.5 km. It is unlikely that the impact of an object of this size would have excavated a crater on the ocean floor (*10*) and this minimum estimate is consistent with the absence of a substantial crustal component in the impact melt (*2*). The estimated maximum size of the asteroid is not much larger. Only for low entry angles (<15°) could asteroids larger than 1 to 2 km avoid excavating a crater in a 5-km deep ocean basin.

Because asteroids with diameters ≥1 km have a probability of impacting Earth every 0.4 million years (*11*), this may have been one of the largest terrestrial impacts since the late Pliocene. However, three impacts of comparable size are known within this time period—the impact events at 0.8 and 1.1 Ma that created the Australasian and Ivory Coast tektites and the Zhamanshin crater impact at ~0.75 Ma (*12*). The Ivory Coast tektites are associated with the 10-km-diameter Lake Bosumtwi impact crater (*13*). Both the Bosumtwi and Zhamanshin craters, the latter also having a diameter of 10 km, require projectiles with a radius of approximately 0.5 km.

An impact of this magnitude must have had a devasting effect on the local environment and could have even had a global influence. The only stratigraphic evidence that may indicate physical disturbance is a major disconformity in E13-4 immediately below the impact horizon (*6*). Although, in contrast to the KT event, this impact is not associated with mass extinctions, the ~2.3 Ma age does correlate with a major deterioration of the late Pliocene climate.

Loess deposits in central China mark the onset of Northern Hemisphere glaciation by a shift from warm, humid environments to cold, dry climates typical of the Pleistocene. Kukla (*14*) pointed out that the glaciation is coincident with a shift in the marine oxygen isotope record, and the approximate magnetostratigraphic age is ~2.36 Ma. The best estimate of the age of the late Pliocene impact on the basis of the magnetic stratigraphy for E13-3 (*15*) is ~2.3 Ma, unresolvable from the onset of glaciation.

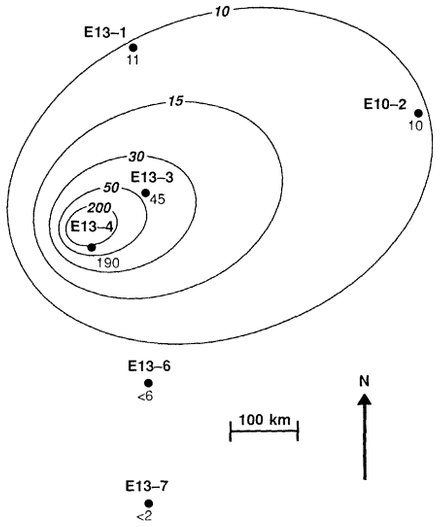

Fig. 3. A model of the fallout distribution on the basis of the net Ir fluences (in nanograms per square centimeter) for six *Eltanin* cores.

Impacts of kilometer-sized asteroids are relatively common, and such events do not always cause climatic shifts. However, it is possible that 2.3 million years ago the Milankovitch cycle had set the environmental stage for the onset of glaciation. This impact probably injected at least 2×10^{15} g of water into the stratosphere (*16*), an amount equal to the current total water content of the stratosphere. Injection of a large fraction of the water to altitudes of 30 km or more may have been sufficient to saturate the upper stratosphere and cause global high-altitude clouds. Perhaps the resulting increase in Earth's albedo was sufficient to produce a rapid decrease in the global temperature, and within a single season to increase significantly the fraction of the continents covered by snow.

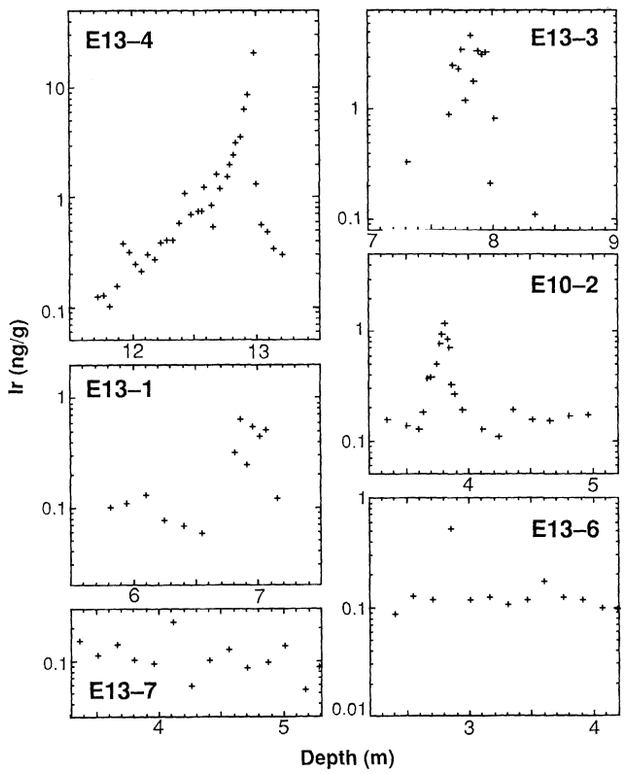

Fig. 2. Iridium profiles across the impact horizons in the six cores. Data for E13-3 are from Kyte *et al.* (*1*). The absence of high Ir concentrations in E13-6 and E13-7 probably reflects low fallout at these sites, but we cannot rule out the possibility of a disconformity at the appropriate level (*6*).

REFERENCES AND NOTES

1. F. T. Kyte, Z. Zhou, J. T. Wasson, *Nature* **292**, 417 (1981).
2. F. T. Kyte and D. E. Brownlee, *Geochim. Cosmochim. Acta* **49**, 1095 (1985).
3. All upper Pliocene sediments in this study are muddy diatomaceous oozes. The analyzed parts of the cores were selected to contain the diatom *Coscinodiscus kolbei*, a species living during the appropriate period [R. M. Weaver and A. M. Gombos, *Soc. Econ. Paleontol. Mineral. Spec. Publ. 32* (1981), p. 445]. Core E13-4 was sampled continuously. Cores E10-2, E13-1, E13-6, and E13-7 were initially sampled at 5-cm intervals, and Ir was analyzed in two or three combined samples, thus spanning 10 to 15 cm. Core E10-2 was reanalyzed in new continuous samples across the Ir-rich interval determined from the survey. Six samples from E13-1 were reanalyzed for Ir at 5-cm intervals. Because cores E13-6 and E13-7 did not have high Ir concentrations, they were not investigated further.

4. Iridium was chemically purified by fusion in Na_2O_2, conversion to chlorides, adsorption onto Srafion NMRR resin [R. A. Nadkarni and G. H. Morrison, *Anal. Chem.* **46**, 232 (1974)], and elution with NH_4OH. Yields were determined by reactivation.
5. All samples from E13-4 were sieved at 420 μm, and seven samples around the horizon were sieved at 149 μm. Selected samples of the other sections were sieved at 149 μm. Coarse fractions were examined microscopically for the presence of impact melt debris, and its presence was confirmed by electron microprobe analyses.
6. Disconformities are common in sediments at this latitude [M. T. Ledbetter and P. F. Cielsielski, *Mar. Geol.* **46**, 329 (1982)]. A large disconformity in E13-4 occurs immediately below the impact horizon. Sediments below this disconformity are Eocene zeolitic nannofossil oozes. Our stratigraphic control is insufficient to rule out the possibility that erosion removed the impact horizon from E13-6 and E13-7.
7. The enhanced Ir in E13-1 most likely shares the same impact source as the other cores, but because we did not recover any particles we were unable to confirm that this is the case.
8. J. P. Kennett, *J. Geophys. Res.* **82**, 3843 (1977).
9. C. Junge, *Air Chemistry and Radioactivity* (Academic Press, New York, 1963); S. Glasstone and P. J. Dolan, *The Effects of Nuclear Weapons* (U.S. Department of Defense, Washington, DC, 1977).
10. For vertical incidence and plausible velocities of 15 to 25 km/s, water depths of 10 to 15 times an asteroid diameter are required to bring the projectile to rest [J. D. O'Keefe and T. J. Ahrens, *Lunar Planet. Sci.* **12**, 785 (1981); *Geol. Soc. Am. Spec. Pap. 190* (1982), p. 103], and the 5-km ocean depth in this region was probably sufficient to prevent the excavation of a crater. The ratio of penetration depth to projectile mass would be lower if the projectile were crushed during atmospheric transit [H. J. Melosh, *Proc. Lunar Planet. Sci. Conf.* **A12**, 29 (1981)]. Another important consideration is the production of shock-vaporized steam [H. J. Melosh, *Geol. Soc. Am. Spec. Pap. 190* (1982), p. 121], which can shield a projectile from the oceanic lithosphere and can eject water vapor and meteoritic material high into the atmosphere.
11. G. W. Wetherill and E. M. Shoemaker, *Geol. Soc. Am. Spec. Pap. 190* (1982), p. 1.
12. R. A. F. Grieve, *Annu. Rev. Earth Planet. Sci.* **15**, 245 (1987).
13. B. P. Glass, *Introduction to Planetary Geology* (Cambridge Univ. Press, New York, 1982).
14. G. Kukla, *Quat. Sci. Rev.* **6**, 191 (1987).
15. J. D. Hays and N. D. Opdyke, *Science* **158**, 1001 (1967).
16. T. J. Ahrens and J. D. O'Keefe, *J. Geophys. Res.* **88**, A799 (1983).
17. We are indebted to A. Kaharoeddin for the diatom survey. Curation of Eltanin cores is supported by the National Science Foundation. This research was supported by Office of Naval Research grant N00014-87.

16 February 1988; accepted 11 May 1988

Velocity of Sound and Equations of State for Methanol and Ethanol in a Diamond-Anvil Cell

J. M. BROWN, L. J. SLUTSKY, K. A. NELSON, L.-T. CHENG

The adaptability of laser-induced phonon spectroscopy to the determination of acoustic velocity and the equation of state in the diamond-anvil high-pressure cell is demonstrated. The technique provides a robust method for measurements at high pressure in both solids and liquids so that important problems in high-pressure elasticity and the earth sciences are now tractable. The velocity of sound and the density of methanol at 25°C have been measured up to a pressure of 6.8 gigapascals. These results imply a higher density (by approximately 5 percent) for liquid methanol above 2.5 gigapascals than that given in existing compilations. The adiabatic bulk modulus increases by a factor of 50 at a maximum compression of 1.8. The thermodynamic Grüneisen parameters of methanol and ethanol both increase with increasing pressure, in contrast to the behavior of most solids.

THE COMPRESSION OF MATERIALS AT high pressure allows the study of interatomic interactions in a regime of distances not otherwise easily accessible. Acoustic velocities are directly related to interatomic force constants and these velocities of sound per se are a matter of central importance in the earth sciences. Knowledge of these properties is essential in any chain of reasoning that proceeds from a seismological image of the earth's interior to a geophysical model in terms of density, temperature, and chemical composition. For solids, compression can be determined by x-ray diffraction although determination of acoustic velocity at very high pressure remains difficult. In the case of liquids and glasses the extended range of pressure and temperature available in the diamond-anvil high-pressure cell has not been extensively exploited for equation of state studies. Laser-induced phonon spectroscopy (*1–3*) offers an approach to the determination of the dynamical mechanical properties and the equation of state of a crystal or fluid well adapted to the requirements of the diamond-anvil cell. We report a determination of the velocity of sound and the equation of state of liquid methanol from ambient pressure to 6.8 GPa. The pressure dependence of the adiabatic compressibility and the thermodynamic Grüneisen parameter of ethanol have also been determined. We believe that the method described here will, with some generality, permit investigation of properties of both crystals and fluids, previously accessible with great difficulty, at very high compressions.

J. M. Brown, Geophysics Program, and L. J. Slutsky, Department of Chemistry, University of Washington, Seattle, WA 98195.
K. A. Nelson and L.-T. Cheng, Department of Chemistry, Massachusetts Institute of Technology, Cambridge, MA 02139.

The geometry of the experiment is illustrated schematically in Fig. 1. A single 1064-nm pulse, 70 ps in duration, is selected from the output train of a continuously pumped Q-switched and mode-locked Nd-YAG laser and split to create two excitation pulses. These pulses are recombined in the sample. The interference of the intersecting excitation pulses in a nonabsorbing sample results in a spatially periodic stress exerted through electrostriction (impulsive stimulated Brillouin scattering) on the sample. The material response to this spatially periodic, temporally impulsive stress is an acoustic standing wave. If there is an appreciable optical absorption coefficient and rapid radiationless decay of the excited state, sudden spatially periodic heating and thermal expansion (impulsive stimulated thermal scattering) can launch counter-propagating acoustic waves that also contribute to the acoustic amplitude. In methanol and ethanol the thermal pressure generated by the weak absorption associated with the third overtone of the CH stretching mode is the

Table 1. Velocity of sound, density, adiabatic compressibility, and thermodynamic Grüneisen parameters of methanol and ethanol as a function of pressure at 25°C.

P (GPa)	Velocity (km/s)	ρ (gm/cm^3)	K_S (GPa)	γ
		Methanol		
0.0001	1.10	0.787	0.96	0.56
0.014	1.18	0.797	1.12	0.60
0.028	1.25	0.808	1.27	0.64
0.041	1.31	0.819	1.41	0.66
0.056	1.37	0.829	1.55	0.68
0.069	1.42	0.836	1.68	0.69
0.083	1.47	0.844	1.82	0.70
0.096	1.51	0.851	1.94	0.71
1.20	2.72	1.074	7.92	0.96
2.07	3.50	1.153	14.20	1.25
2.58	3.76	1.196	16.91	1.35
2.59	3.76	1.196	16.90	1.35
2.92	3.84	1.221	18.03	1.43
4.06	4.53	1.290	26.48	
4.30	4.77	1.303	29.64	
4.89	5.10	1.329	34.69	
6.32	5.53	1.383	42.23	
6.52	5.87	1.390	47.93	
6.82	5.77	1.400	46.57	
		Ethanol		
0.0001	1.15	0.785	1.03	0.59
0.58	2.09	0.983	4.29	0.75
1.32	2.86	1.085	8.88	0.99
1.35	3.08	1.087	10.3	1.14
1.90	3.39	1.138	13.0	1.16
2.12	3.40	1.158	13.7	1.12
2.20	3.57	1.165	14.8	1.17
3.19	3.97	1.241	19.6	1.17